Monitoring the surface inflow of Atlantic Water to the Norwegian Sea using Envisat ASAR

M. W. Hansen,[1] J. A. Johannessen,[1,2] K. F. Dagestad,[1] F. Collard,[3] and B. Chapron[4]

Received 9 June 2011; revised 13 August 2011; accepted 12 September 2011; published 7 December 2011.

[1] Sea surface range Doppler velocities from nearly 1200 Envisat Advanced Synthetic Aperture Radar (ASAR) acquisitions between 2007 and 2011, covering the Norwegian Sea, the North Sea, and the Skagerrak Sea, have been examined. After systematic corrections, the inflow of Atlantic Water to the Norwegian Sea, via the two branches of the Norwegian Atlantic Current, is investigated. Distinct expressions of the eastern branch, the Norwegian Atlantic Slope Current, are revealed with a speed of 20–40 cm/s and a clear manifestation of topographic steering along the 500 m isobath. The western branch, the Norwegian Atlantic Front Current, is also depicted but with lower surface velocities. Moreover, parts of the Norwegian Coastal Current are also detected with time-averaged speed reaching up to 40 cm/s. At a spatial resolution of 10 km, the root mean square errors of these velocities are estimated to be less than 5 cm/s. The range Doppler velocity retrievals are assessed and compared to other direct and indirect estimates of the upper ocean current, including surface Lagrangian drifters, moored recording current meter measurements, and surface geostrophic current inverted from several mean dynamic topography fields. The results are promising and demonstrate that the synthetic aperture radar based range Doppler velocity retrieval method is applicable to monitoring the temporal and spatial variations of ocean surface circulation, provided the imaging geometry is favorable.

Citation: Hansen, M. W., J. A. Johannessen, K. F. Dagestad, F. Collard, and B. Chapron (2011), Monitoring the surface inflow of Atlantic Water to the Norwegian Sea using Envisat ASAR, *J. Geophys. Res.*, *116*, C12008, doi:10.1029/2011JC007375.

1. Introduction

[2] The transport of warm and saline Atlantic Water (AW) into the Nordic Seas with the Norwegian Atlantic Current (NwAC) is of great importance for the high-latitude and Arctic ocean circulation regime, climate, and ecosystem. The NwAC is composed of two branches [e.g., *Poulain et al.*, 1996; *Orvik et al.*, 2001; *Søiland et al.*, 2008] referred to as the Norwegian Atlantic Slope Current (NwASC) [*Skagseth and Orvik*, 2002] and the Norwegian Atlantic Front Current (NwAFC) [*Mork and Skagseth*, 2010] (see Figure 1). The NwASC, originating mainly from the Faroe-Shetland channel, is near barotropic and steered by topography along the southeastern domain of the Norwegian Sea. The baroclinic NwAFC is linked to the Arctic Front (the transition zone between the Atlantic and Arctic water in the Nordic Seas) and enters over the Iceland-Faroe Ridge as the Faroe Current. The variations in the NwASC is strongly linked to both the local and the large scale wind field [e.g., *Gordon and Hithnance*, 1987; *Skagseth and Orvik*, 2002; *Orvik et al.*, 2001; *Orvik and Niiler*, 2002; *Skagseth et al.*, 2004], while the tidal signal is rather weak around 2–3 cm/s [*Orvik et al.*, 2001]. In contrast, little is known of the forcing and variability of the NwAFC [*Mork and Skagseth*, 2010], although it is highly dominated by mesoscale eddy activity [see, e.g., *Nilsen and Nilsen*, 2007; *Søiland et al.*, 2008, and references therein].

[3] Combined with the advanced quantitative knowledge of the marine geoid at scales from 200 to 500 km that has emerged from gravity missions, e.g., the Gravity Recovery and Climate Experiment (GRACE) and the Gravity Field and Steady State Ocean Circulation Explorer (GOCE), in recent years [*Maximenko et al.*, 2009], we can now derive mean dynamic topography (MDT) from the time varying signal from altimetry, as well as surface drifters and other in situ measurements, to reconstruct the absolute surface geostrophic current. Using MDT in combination with hydrographic data, *Hunegnaw et al.* [2009] and *Mork and Skagseth* [2010] recently estimated the transport in the NwASC across the Svinoy section (Figure 1) to about 3.9 Sv (temporal mean between 1993 and 1996) and 3.4 ± 0.3 Sv (temporal mean between 1992 and 2009), respectively. In comparison *Orvik et al.* [2001] and *Orvik and Skagseth* [2003] estimated the mean transport in the NwASC to 4.2 Sv and 4.4 Sv, respectively, using moored recording current meters (RCMs) in combination with hydrographic data.

[1]Nansen Environmental and Remote Sensing Center, Bergen, Norway.
[2]Geophysical Institute, University of Bergen, Bergen, Norway.
[3]Collecte Localisation Satellites, Plouzané, France.
[4]Laboratoire d'Océanographie Spatiale, Institut Francais de Recherche pour l'Exploitation de la Mer, Plouzané, France.

0148-0227/11/2011JC007375

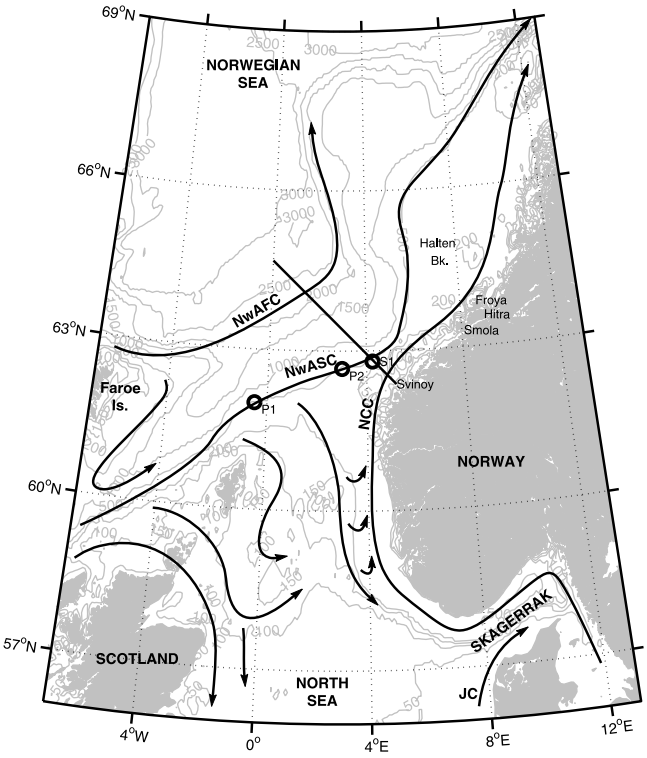

Figure 1. Schematic of the general ocean circulation in our area of interest. Isobaths are drawn for every 50 m to 200 m and every 500 m from 500 m. The marked straight line indicates the Svinoy section. P1, P2, and S1 are points of reference used in the text. Other abbreviations are as follows: JC, Jutland Current; NT, Norwegian Trench; NCC, Norwegian Coastal Current; NwASC, Norwegian Atlantic Slope Current; NwAFC, Norwegian Atlantic Front Current.

[4] In complement, new techniques have emerged which permit a direct retrieval of line-of-sight (range) surface velocity fields from Synthetic Aperture Radar (SAR) [*Romeiser et al.*, 2010] without the need to rely on the geostrophic assumption. One technique, along-track interferometry (ATI), requires a second receiving antenna (or a split antenna) [*Goldstein and Zebker*, 1987], while the single antenna range Doppler velocity method enables estimates from conventional SAR raw data at a reduced spatial resolution [*Chapron et al.*, 2005; *Johannessen et al.*, 2008; *Rouault et al.*, 2010]. These complementary observations have a clear potential to strengthen the ability to study temporal and spatial variability of ocean surface currents.

[5] In this paper, we investigate the capability of the single antenna range Doppler velocity method for mapping the inflow of AW to the southern Norwegian Sea and the Skagerrak Sea. The speed of this surface current is about 20–50 cm/s [e.g., *Orvik et al.*, 2001] and clearly weaker than the Agulhas Current and Gulf Stream, which have velocities up to 2 m/s [e.g., *Bryden et al.*, 2005] and for which the range Doppler velocity method has been shown to give reliable estimates [*Chapron et al.*, 2005; *Johannessen et al.*, 2008; *Rouault et al.*, 2010]. In our focus area (Figure 1), however, it is expectedly more challenging to separate the range Doppler velocity from uncorrected errors in the image product, and averaging is required to improve the signal-to-noise ratio. This method was successfully demonstrated by *Rouault et al.* [2010] for the Agulhas region.

[6] The method used for retrieving the range Doppler velocity from the Envisat Advanced Synthetic Aperture Radar (ASAR) Wide Swath Medium resolution image (WSM) product in VV polarization is briefly addressed in section 2.1, followed by a detailed presentation of the results in section 2.2. In section 3 we examine the quality and reliability of the results by comparison to other direct and indirect estimates of surface current. In section 4 we provide the summary and conclusions.

2. Sea Surface Range Doppler Velocity From Envisat ASAR

2.1. Method

[7] ASAR is a side-looking synthetic aperture radar which operates in C-band on board the European Space Agency (ESA) polar orbiting satellite Envisat. In Wide Swath mode, it spans a range of incidence angles from 16° to 43° relative to the surface normal, with a swath width of 420 km. Since mid 2007, a grid of Doppler centroid frequencies, f_{Dc} [*Madsen*, 1989], is included in the ASAR WSM level-1b products. The cross-track pixel spacing is about 9 km in near range and 3.5 km in far range, while the pixel spacing in the azimuth direction is fixed at about 8 km. Estimates of a geophysical Doppler shift, f_g, can be obtained by subtracting a predicted Doppler shift, f_{Dp}, based on precise knowledge of the satellite orbit and attitude, from the Doppler centroid frequency estimate, f_{Dc} [*Chapron et al.*, 2005]. The geophysical Doppler shift, f_g, relates to a spatial mean of the range component, v_r, of the velocity of the surface scattering elements, weighted by the local normalized radar cross section (NRCS) (σ_0) [*Romeiser and Thompson*, 2000; *Chapron et al.*, 2005] as

$$f_g = -\frac{k_e V_D}{\pi} = -\frac{k_e}{\pi}\frac{\overline{v_r \sigma_0}}{\overline{\sigma_0}}, \tag{1}$$

where k_e (112 m^{-1} for ASAR) is the electromagnetic wavenumber, V_D is by definition the line-of-sight range Doppler velocity, and the overbars characterize spatial averaging. The line-of-sight velocity, v_r, of the scattering elements is here defined positive for motion toward the radar in descending pass and away from the radar in ascending pass (i.e., always positive for motion in the easterly direction). The range Doppler velocity is thus a result of the line-of-sight velocities of all surface scattering elements, including Bragg resonance waves, specular facets (mirror points), and breaking waves, advected by and interacting with any underlying surface current [see, e.g., *Chapron et al.*, 2005; *Johannessen et al.*, 2008]. A comprehensive description of the processing steps and error corrections needed to retrieve estimates of f_g, and thus V_D, from Envisat ASAR WSM products is presented by *Hansen et al.* [2011]. The instrumental accuracy, expressed as the root mean square error (RMSE), of the observed geophysical Doppler shift is found to be $\epsilon_f \approx 5$ Hz for a single scene in VV polarization. This corresponds to an instrumental accuracy of the horizontally projected range Doppler velocity ($V_{Dh} = V_D/\sin\theta$) of about 20 cm/s at incidence angle $\theta = 40°$ and 40 cm/s at $\theta = 20°$.

[8] We have retrieved geophysical Doppler shifts (f_g) from nearly 1200 ASAR WSM acquisitions in VV polarization between August 2007 and February 2011. These are corrected for the local contribution, f_w, from the wind using the CDOP model developed by *Collard et al.* [2008] and A. A. Mouche et al. (On the use of Doppler for sea surface wind retrieval from SAR, submitted to *IEEE Transactions on Geoscience and Remote Sensing*, 2011). These local wind contributions are mainly from wave orbital motion but also from Ekman and Stokes drift. The range Doppler velocity calculated from the corrected Doppler shift is assumed to be a measure of the surface current (in the horizontal plane) according to

$$V_c = -\frac{\pi(f_g - f_w)}{k_e \sin\theta}. \quad (2)$$

Consequently, any errors in the wind field estimate (both speed and direction) add to the uncertainty of f_g. Note also that large incidence angles are more favorable, since a larger fraction of the horizontal velocity is directly detected. The wind field invoked to CDOP is in this study retrieved from the global forecasting system of the (US) National Center for Environmental Prediction (NCEP) at a 3 hourly basis with a latitudinal and longitudinal grid size of 0.5°. As the model wind direction estimates at low wind speed are more uncertain, the ASAR range Doppler velocity data in our analysis is discarded for winds weaker than 4 m/s. By assuming errors in the NCEP wind speed and direction of 2 m/s and 15°, respectively, CDOP is used to find a maximum error, ϵ_w, of the wind related Doppler shift, which is added to the instrumental accuracy. This gives an error in the wind corrected range Doppler velocity of $\epsilon_v = \left|\pi\sqrt{\epsilon_f^2 + \epsilon_w^2}/k_e \sin\theta\right|$. The wind corrected range Doppler velocities and associated error estimates are then spatially interpolated to a grid of 5 × 5 km^2 pixels. Finally, temporal averages are calculated by weighting the gridded wind corrected range Doppler velocity estimates, $V_{c,i}(t_j)$, by the inverse of their error variances, $\epsilon_{V,i}(t_j)^2$, expressed as [*Taylor*, 1997]

$$\mu_i = \frac{\sum_j \left(V_{c,i}(t_j)/\epsilon_{v,i}(t_j)^2\right)}{\sum_j \left(1/\epsilon_{v,i}(t_j)^2\right)}, \quad (3)$$

with associated error variance

$$\epsilon_{\mu,i}^2 = \frac{1}{\sum_j \left(1/\epsilon_{v,i}(t_j)^2\right)}, \quad (4)$$

where i and j are spatially and temporally distributed samples, respectively. Since the ASAR sampling is irregular in time, the temporal averages are first found on a weekly basis and then over longer time spans using the weekly values. Because of the different radar look directions, data from ascending and descending tracks must be averaged separately.

2.2. Results

[9] Following the procedure presented in section 2.1, the weighted mean (August 2007 to July 2010) wind corrected range Doppler velocity over the southeast Norwegian Sea and northern part of the North Sea is shown in Figure 2. In ascending and descending satellite pass, positive velocity is toward 77° and 103°, respectively, measured clockwise relative to north as indicated by the arrows. It should be noted that the two fields represent conditions at different times of the day, around 08:00 and 20:00 local solar time for descending and ascending pass, respectively. Each data point is an average of at least 50 observations as seen in Figures 2c and 2d. At the spatial resolution of 10 km, the corresponding weighted RMSE (equation (4)) is found to be less than 8 cm/s in regions of more than 100 observations and 4–5 cm/s in regions of more than 150 observations. This wind corrected range Doppler velocity is thus expected to represent the mean surface current of the inflowing AW multiplied by the cosine of the difference between the true current direction and the ASAR range direction. The configurations are thus unfavorable for current flowing in the north–south direction, as only small range components will be detected.

[10] In both the ascending and descending wind corrected range Doppler velocity maps, the NwASC is evidently steered along the 500 m depth contour. Between the points P1 (62°N, 0°30′W) and S1 (62°48′N, 4°15′E) shown in Figure 1, the ascending pass configuration is optimum with the range direction nearly aligned with the mean orientation of the isobaths and the inflowing AW. The width (full width at half maximum) of the current is 60 km at P1, then decreases to 45 km at P2 (62°40′N, 3°E) where it aligns with the Norwegian Coastal Current (NCC), before it increases again to 60 km at S1 in the Svinoy section. Note that the velocity profile across the latter, however, now describes the combined surface drift of the NwASC and the NCC, and that we are not able to automatically separate these signals with ASAR. However, the western edge of the NCC (Figure 2, especially in descending pass) appears to follow the slope slightly west of the 200 m isobath in the eastern sector of the Norwegian Trench (NT) in a northwesterly direction toward P2. In turning toward east, the western edge of the NCC may be expected to maintain the tendency of following this isobath. Using the 200 m isobath as the limit between the NCC and the NwASC, the mean width of the NwASC at the Svinoy section is thus found to be 36 km. The central wind corrected range Doppler velocity varies from 40 cm/s at P1, via a minimum of 20 cm/s at P2 to 30–35 cm/s at the Svinoy section. These estimates and the evidence of topographic steering are in general agreement with, for example, *Orvik et al.* [2001], *Søiland et al.* [2008], and *Mork and Skagseth* [2010].

[11] The NwAFC is evident in the ascending pass velocity map north of the NwASC as a broad band of surface velocities of about 15 cm/s following the depth contours from 2000 m to 2500 m in the northwest and gradually reducing toward 10 cm/s at the interception of the Svinoy section (Figure 2a). The latter wind corrected range Doppler velocity is also encountered in the descending pass as noticed in Figure 2b. East of the Svinoy section, the depth contours become more north–south oriented, and the current signatures of both the NwASC and the NwAFC become correspondingly weaker (less than 10 cm/s) in both ascending and descending configuration. At about 66°N, 6°E the NwASC again turns into a more favorable easterly direction,

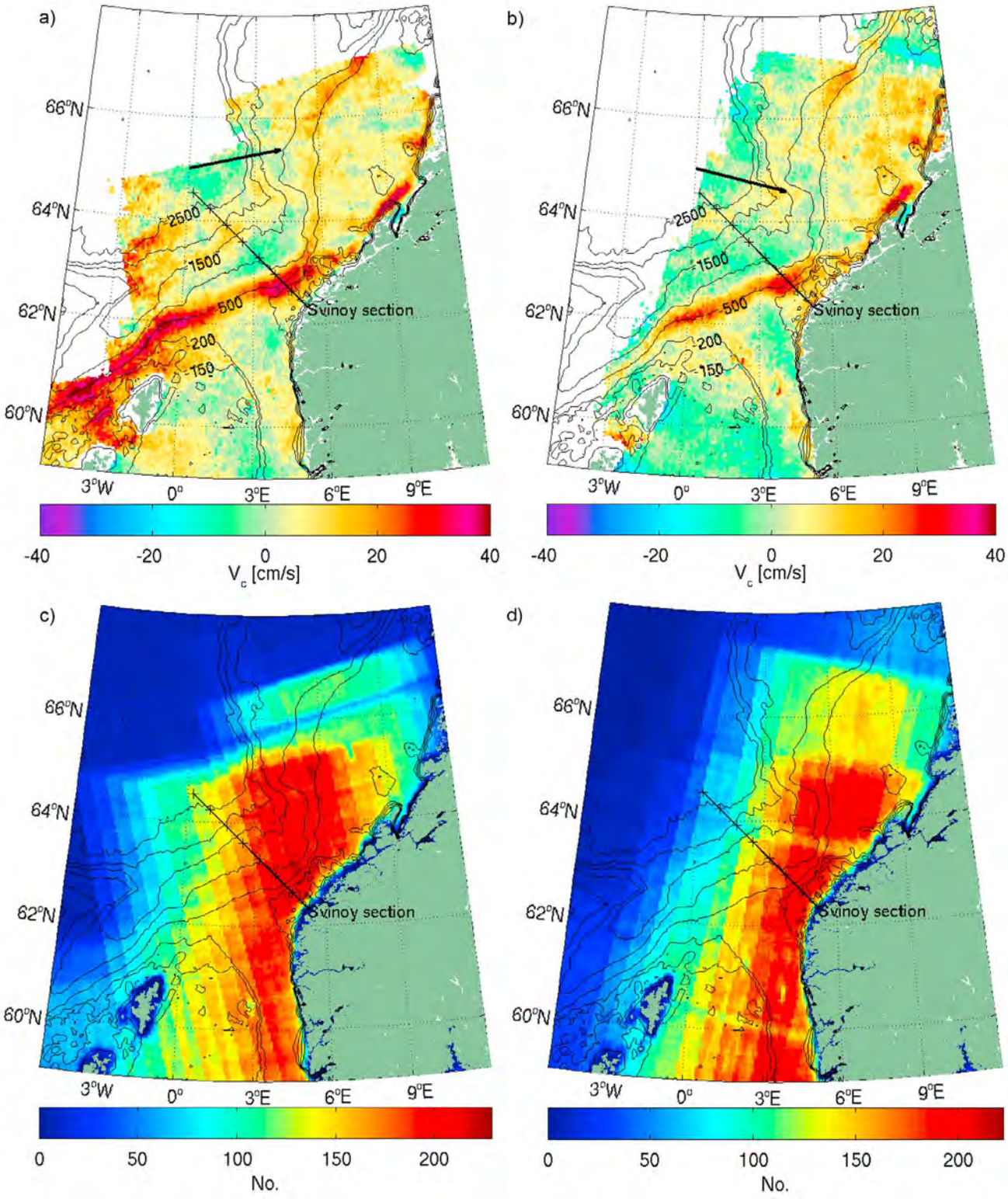

Figure 2. Mean (August 2007 to July 2010) ASAR WSM sea surface wind corrected range Doppler velocity (VV polarization) in (a) ascending and (b) descending pass over the northern North Sea and the Norwegian Sea. The values are positive for any flow component within 90° from the direction indicated by the arrows. Also shown is the number of ASAR observations per grid point in (c) ascending and (d) descending satellite pass. Each data point at the top contains at least 50 observations, and the pixel size is 5 × 5 km^2. The RMSE is about 5 cm/s in the well-covered areas (>100 observations) and less than 10 cm/s elsewhere. Tick marks along the Svinoy section indicate 50 km intervals.

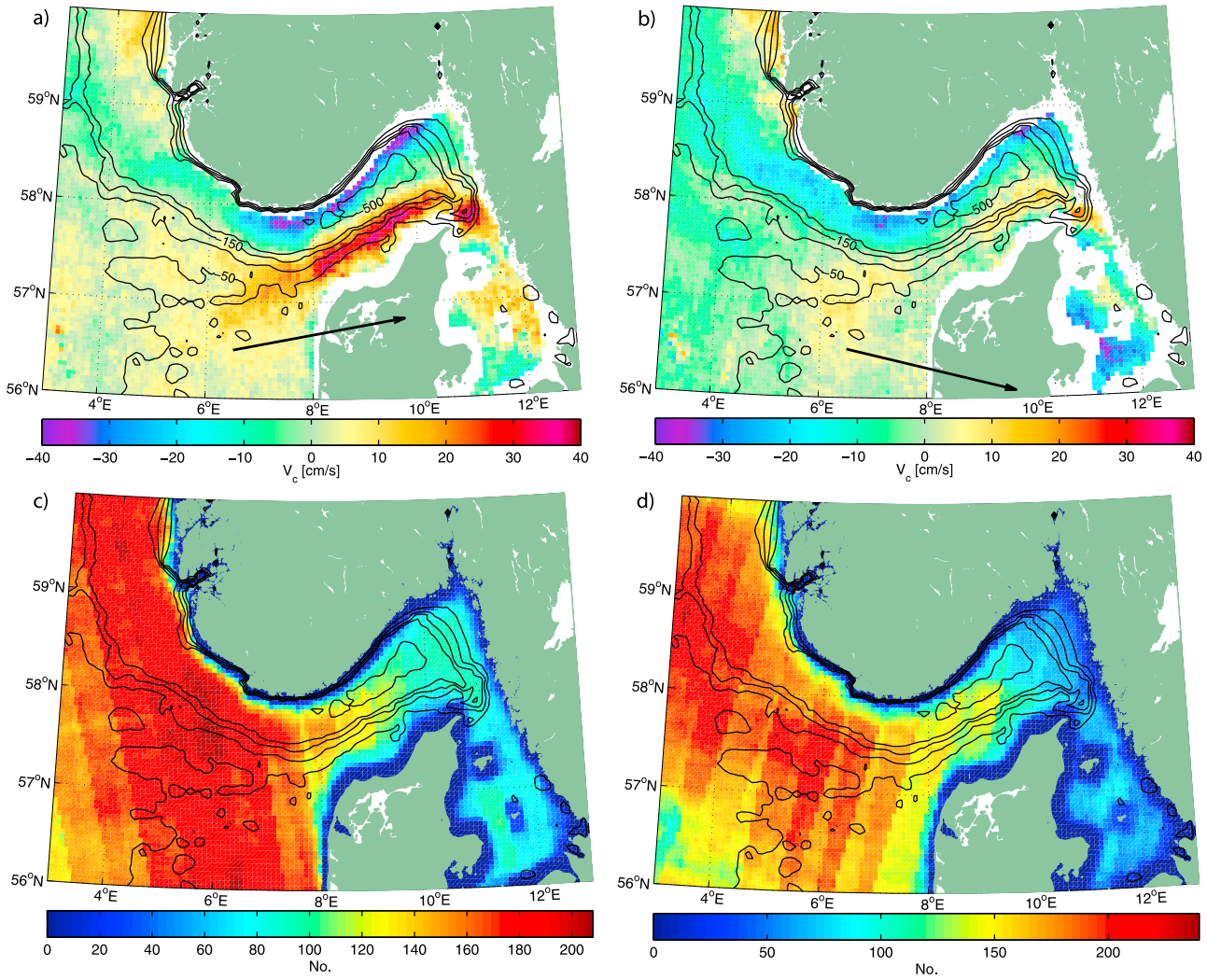

Figure 3. Same as Figure 2, but for the eastern North Sea and Skagerrak.

and thus becomes more visible in the wind corrected range Doppler velocity.

[12] Along the west coast of Norway (south of 62°N in Figure 2), the NCC maintains mostly a northward flow direction, whereas the inflowing AW is steered southward along the 200 m isobath in the western sector of the NT. With such unfavorable geometry, the range Doppler velocities are correspondingly weak. The evidence of some easterly oriented flow of around 10 cm/s in the NT might be connected with recirculation of AW which is known to take place in this region [*Furnes et al.*, 1986]. Further north, on the other hand, the NCC becomes visible as a strong and narrow jet between the Haltenbanken and the Frøya island centered at about 64°N, 9°E. The wind corrected range Doppler velocity in ascending pass is here about 30–40 cm/s with a current width of about 30 km.

[13] The results suggest that the range Doppler velocity method is useful to monitor persistent and topographically trapped currents, provided the imaging geometry is favorable. As such, it might also be feasible to apply the method to detect the general cyclonic circulation in the Skagerrak [*Sætre*, 2007]. As known from the literature, the Jutland Current transports North Sea water along the Danish west coast north-eastward into the Skagerrak where it mixes with southeastward flowing AW. In the eastern part of the Skagerrak, further mixing takes place with the outflow of freshwater from the Baltic Sea. The corresponding mixed water mass defines the origin of the NCC, which in turn flows west-southwestward out of the Skagerrak and continues northward along the coast of Norway as a narrow boundary current. Note that the use of satellite altimetry for ocean current retrieval in this region is limited due to land contamination in the radar resolution cells, and the existence of Lagrangian surface drifters is rare.

[14] The weighted mean wind corrected range Doppler velocity in the eastern North Sea and Skagerrak is shown in Figure 3. The number of observations and corresponding errors are comparable to the best covered areas in Figure 2, except for the lower coverage in the eastern part of Skagerrak where the accuracy approaches only 10 cm/s in descending pass. For the ascending pass, the mean wind corrected range Doppler velocity of the Jutland Current and the NCC reach 40–50 cm/s and 25–30 cm/s, respectively. In the descending pass, the imaging geometry is less favorable in the Skagerrak, and the evidence of the Jutland Current is seen with maximum wind corrected range Doppler velocity

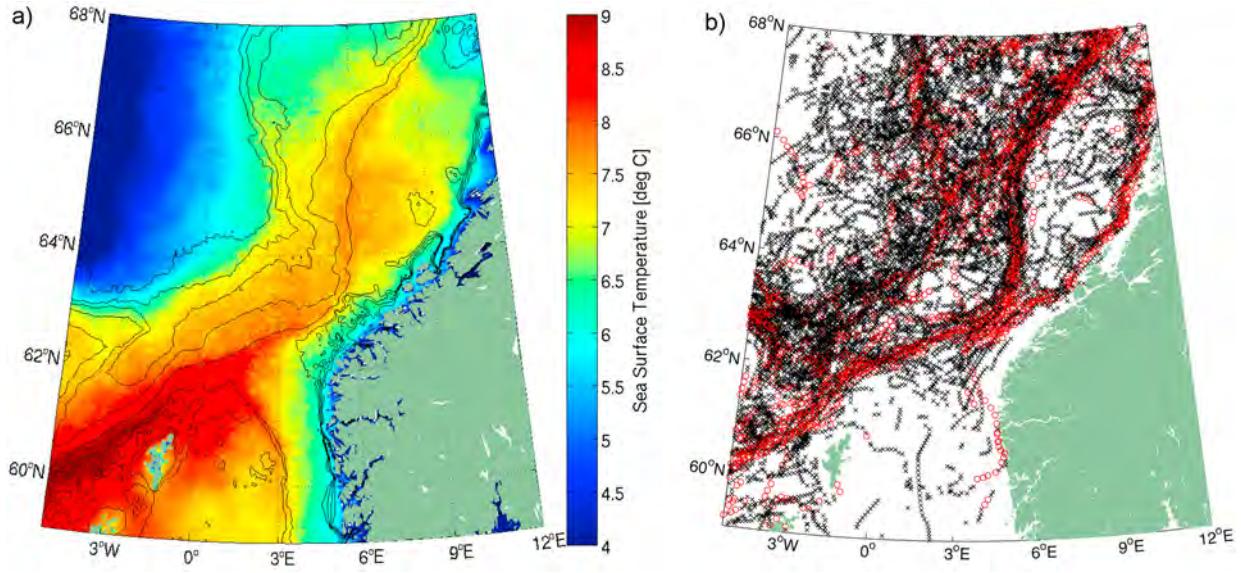

Figure 4. (a) Mean SST in winter (December–February from 2002 to 2011) from monthly MODIS Level-3 data (from the Web site of NASA Goddard Space Flight Center), and (b) the general circulation in the southern Norwegian Sea as manifested by surface Lagrangian drifters during the period 1991–2007 (from the Web site of Fisheries and Oceans Canada (http://www.meds-sdmm.dfo-mpo.gc.ca/)). The black crosses are positions of drifters with speeds between 25 cm/s and 50 cm/s, while the red circles are positions of drifters with speeds greater than 50 cm/s.

reduced to about 10–15 cm/s. The NCC flowing out of Skagerrak, however, is more distinct in the descending pass, with a wind corrected range Doppler velocity of 20–25 cm/s.

[15] As we have averaged wind corrected range Doppler velocities in the two range directions (ascending and descending), a mean two-dimensional vector field can in principle be reconstructed. However, since the angle between the two directions is only 26°, the uncertainty on the vector component in the north–south direction will be too large to give meaningful results. Hence in this paper we restrict the discussion to the range Doppler velocity.

3. Evaluation of Results

[16] From section 2.2 it is clear that the maps of wind corrected range Doppler velocity document the importance of topographic steering. The mean winter (DJF) nighttime sea surface temperature (SST) from satellite in Figure 4a contains similar evidence. Although it does not provide direct estimates of the surface current, the pattern in the SST map qualitatively agree well with the ASAR wind corrected range Doppler velocity as described in the previous section. In addition, the temperature gradient in the winter SST indicates that NCC water occupy the area to the southeast of the 200 m isobath, and that AW dominate the signal further northwest. This supports the previous assumption of a separation between the NwASC and the NCC at the 200 m isobath.

[17] In order to further evaluate these results we use sea surface Lagrangian drifter data, geostrophic current estimates derived from MDT and altimetry, as well as a moored RCM at the position S1 in the Svinoy section (Figure 1). These data sets represent current estimates for different depths of the upper ocean, and have different integration times and spatial resolutions as specified in Table 1.

3.1. Surface Drifter Data

[18] The positions of surface Lagrangian drifters between 1991 and 2007 from the Global Drifter Program (GDP) of the Atlantic Oceanographic and Meteorology Laboratory (AOML) in Miami, Florida, are shown in Figure 4b. The surface Lagrangian drifters represent the current at 15 m depth, and their functionality and water following characteristics are described by *Niiler* [2001] while the quality control and data interpolation is described by *Hansen and Poulain* [1996]. Only the positions of drifters with velocity exceeding 25 cm/s are shown. The positions of both the NwASC and the NwAFC, as well as the NCC north of 62°N, are evident by the Lagrangian drifter positions, and agree well with the wind corrected range Doppler velocity maps in Figure 2. An upper bound for the maximum width of the NwASC is here measured to about 90 km, and the speed reaches more than 50 cm/s whereas the highest speeds in the broader (up to 140 km) NwAFC are generally lower.

Table 1. Summary of Data Sources According to Sampling Period, Grid Size, and Observation Depth

Data	Period	Grid Spacing (km)	Depth
ASAR	2007–2011	5	surface
SST	2002–2011	2	surface
Drifters	1990–2006	100	15 m
CNES-CLS09 MDT	1993–1999	50	surface
GOCINA MDT	1993–1999	4	surface
GOCE MDT	1993–1999	7 × 14	surface
AVISO ADT	2007–2009	30	surface
Svinoy RCM	2007–2010	—	100 m

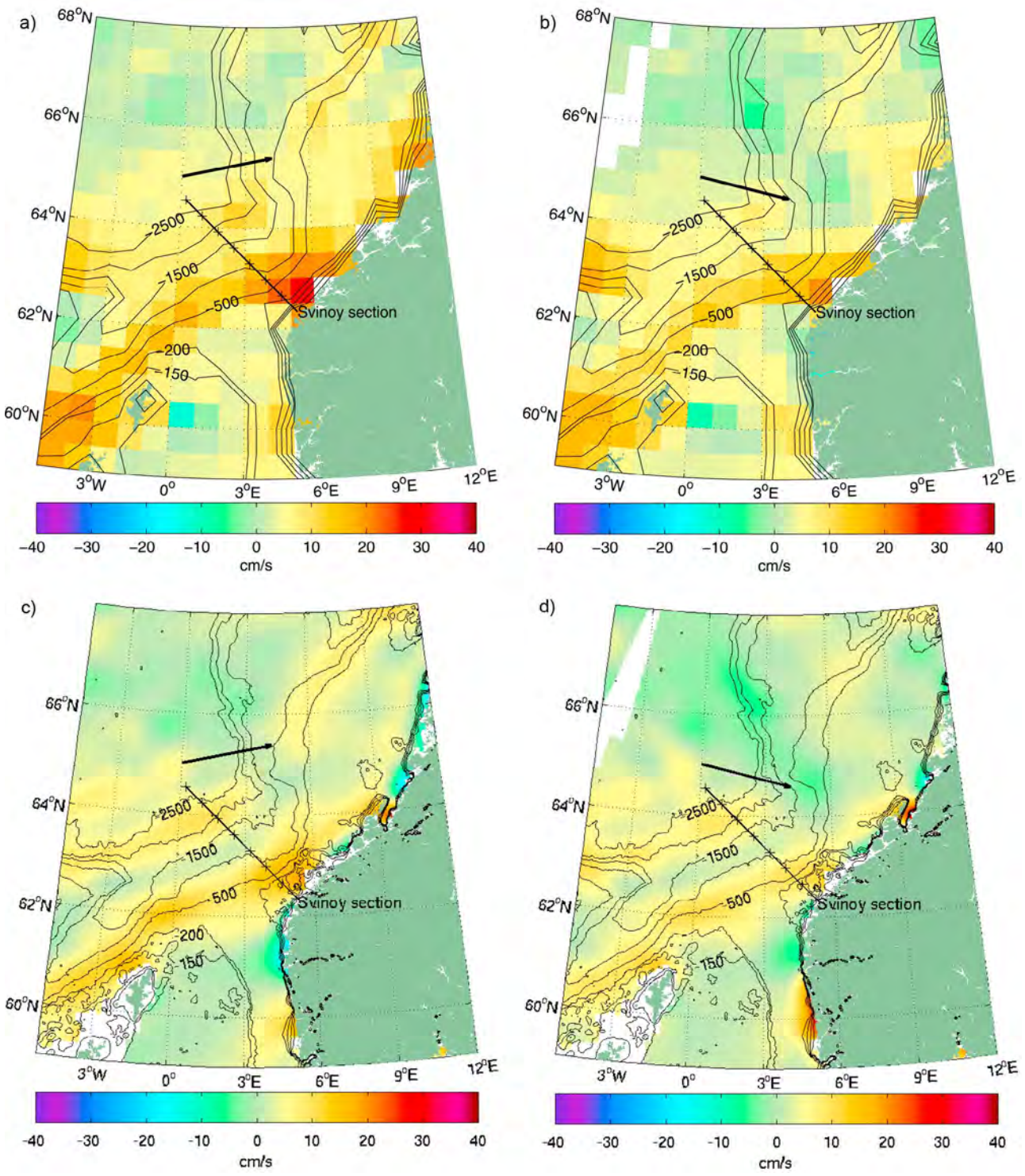

Figure 5. (top) Mean current deduced from surface Lagrangian drifter observations between 1990 and 2006 over the northern North Sea and the Norwegian Sea, and (bottom) geostrophic current associated with the GOCINA MDT over the same region. Both fields are courtesy of *Hunegnaw et al.* [2009] and are projected into the ASAR range direction in (a and c) ascending and (b and d) descending pass configuration.

[19] The gridded surface velocity field obtained by interpolation of surface Lagrangian drifter velocities filtered for nongeostrophic contributions (received from *Hunegnaw et al.* [2009]) and projected into the ASAR ascending and descending pass configuration, is shown in Figures 5a and 5b, respectively. The most evident agreement with the ASAR wind corrected range Doppler velocity (Figure 2) is the tendency of the inflowing NwASC to follow the continental

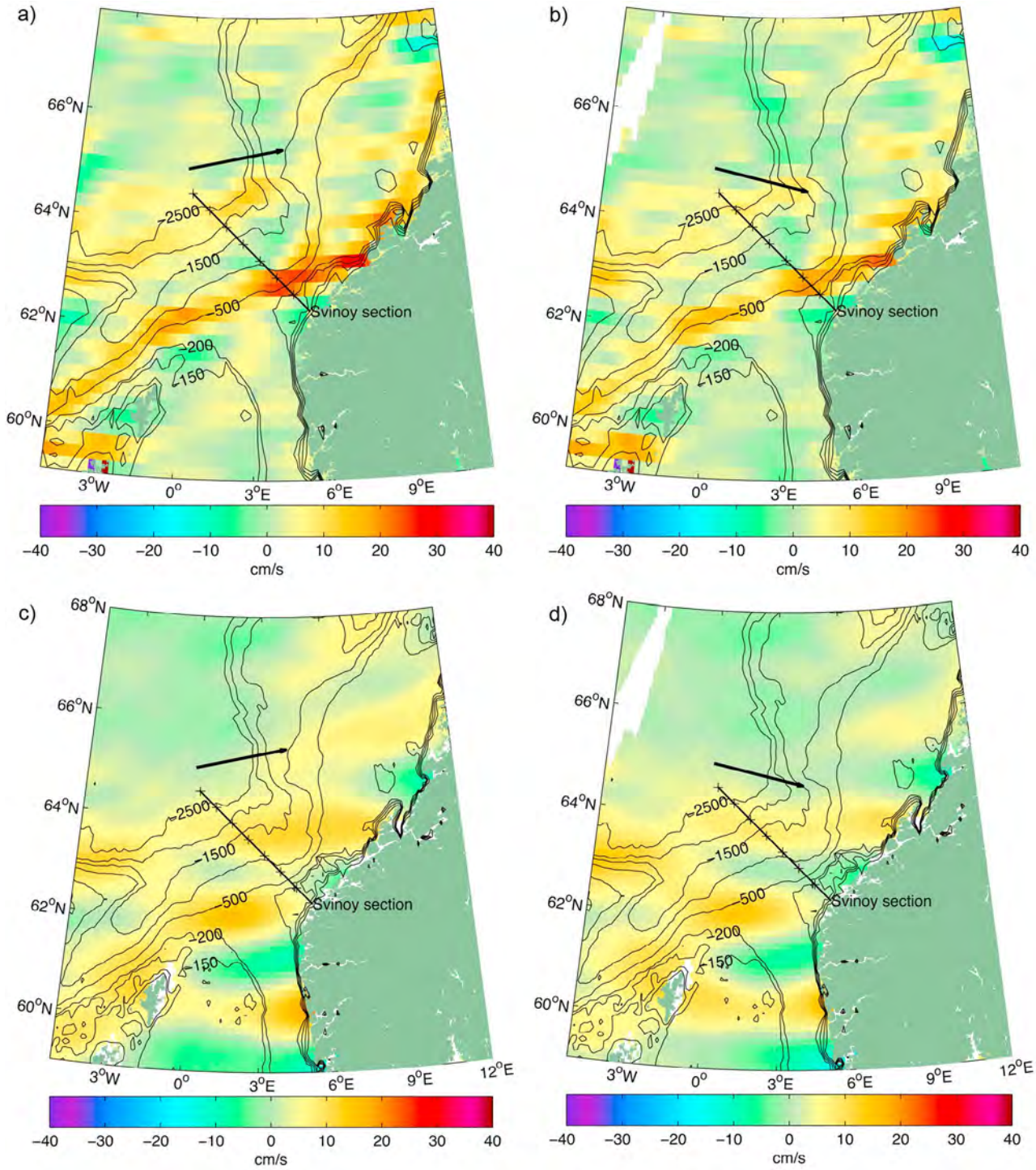

Figure 6. (top) Mean geostrophic currents associated with the CNES-CLS09 and (bottom) preliminary GOCE MDTs, projected to the range direction of ASAR measurements in (a and c) ascending and (b and d) descending pass configuration over the northern North Sea and the Norwegian Sea.

slope along the 500 m depth contour across the southern Norwegian Sea, although the resolution of the mapped drifter velocities (∼200 km) is too low to reveal any of the finer scale variations observed with ASAR. Consequently, the maximum velocities of up to 20 cm/s are also weaker than depicted in the wind corrected range Doppler velocity maps.

3.2. Mean Surface Geostrophic Current

[20] On time scales of a few days or more, and spatial scales of tens of kilometers, the NwAC is generally in geostrophic balance [*Orvik et al.*, 2001; *Hunegnaw et al.*, 2009; *Mork and Skagseth*, 2010]. In this section, we compare the ASAR derived mean sea surface wind corrected range

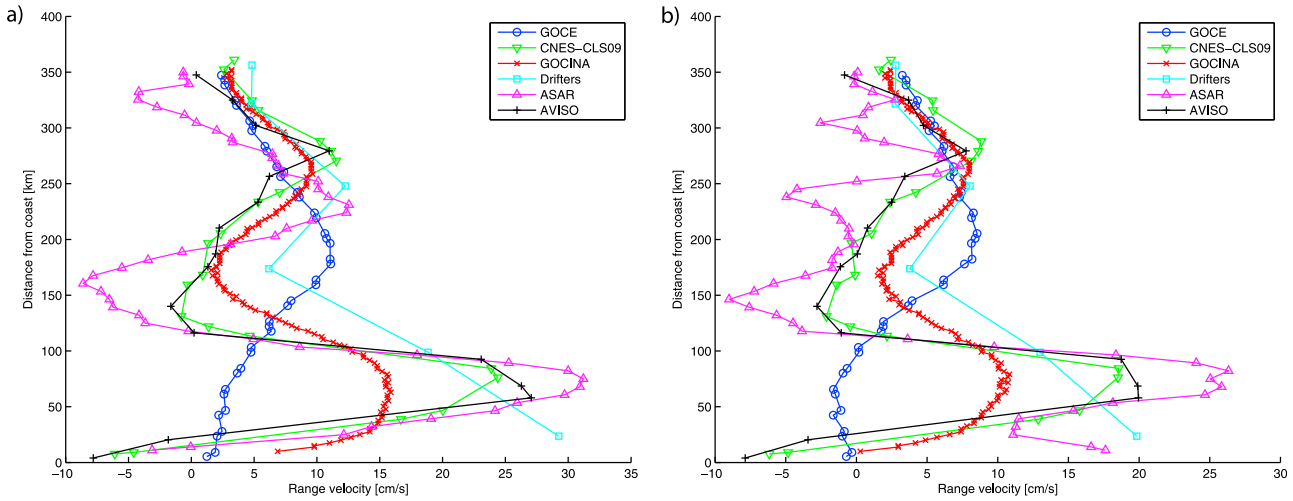

Figure 7. Range velocities across the Svinoy section (see Figure 1) in (a) ascending and (b) descending satellite pass. The AVISO ADT retrievals cover the period from August 2007 to July 2009 because DT MSLA grids were only available until March 2010. The data is extracted from regular longitude/latitude grids which causes irregularity along the vertical axis.

Doppler velocity with the mean sea surface geostrophic current based on MDTs from three sources: (1) Centre National d'Etudes Spatiales (CNES) and Collecte Localisation Satellites (CLS) (CNES-CLS09, *Rio et al.* [2011]); (2) the EU GOCINA project [*Hunegnaw et al.*, 2009]; (3) the preliminary results from GOCE [*Knudsen et al.*, 2011]. The reference period and grid size of these fields are provided in Table 1. To allow direct comparison, the geostrophic velocity fields are projected into the horizontal range direction of the range Doppler velocity data. The geostrophic currents based on the GOCINA (Figures 5c and 5d) and CNES-CLS09 (Figures 6a and 6b) MDTs correspond quite well with the ASAR observations. In particular, the location of the NwASC centered along the 500 m isobath agree well, although its magnitude is significantly larger in ASAR than in CNES-CLS09 and GOCINA which reach up to 25 cm/s and 15 cm/s, respectively. Between P1 and the Svinoy section, the ASAR results give maximum velocities twice as large as those from CNES-CLS09 and four times as large as the GOCINA results. Further north, the general location and pattern of the NwASC also agree well, but the ASAR wind corrected range Doppler velocity is stronger. In comparison, the range geostrophic current inverted from the GOCE MDT (Figures 6c and 6d) appears to contain banded discrepancies at some locations near land around 60°N, 62°N, 64°N, and 66°N. The distance between the discrepancies is about 200 km, which is close to the resolution of GOCE (harmonic degree of 200; *Knudsen et al.* [2011]). It is, however, not the intention to explain the GOCE based results in this paper, although the errors might be connected to inaccuracies in the Mean Sea Surface Height (MSSH) and in the preliminary geoid used to calculate the MDT. Nevertheless, similarities are also seen here, e.g., over the NwAFC with maximum speed of 10–15 cm/s and a region of recirculation between the NwASC and the NwAFC.

[21] The NwAFC is also evident in the velocities calculated from the GOCINA and CNES-CLS09 MDTs. Like with ASAR, this is separated from the NwASC by a region of zero or slightly negative range velocities. The magnitudes seem to correspond better here than in the NwASC, although the ASAR velocities are slightly larger.

[22] The slight disagreement between the ASAR and the MDT based surface velocity retrievals arises from differences in the observing methods. The ASAR range Doppler velocity is related to the total surface motion including non-geostrophic contributions, e.g., surface divergence, Ekman drift, and eddy induced acceleration of the mean current [e.g., *Hughes and Ash*, 2001] and not just the geostrophic velocity. Moreover, as the spatial scale of the eddies in the region is ranging from 20–50 km in diameter [e.g., *Johannessen et al.*, 1996], these will not be properly resolved by the altimetric measurements.

3.3. Mean and Seasonal Flow Across the Svinoy Section

[23] A final quantitative assessment is based on a comparison of the mean flow across the Svinoy section observed with ASAR, gridded drifter velocities, and the three different MDT estimates. In order to compare the ASAR data to the most relevant geostrophic current climatology, we also include results of combined CNES-CLS09 MDT and Delayed Time (DT) Maps of Sea Level Anomalies (MSLA) obtained from altimeter measurements between August 2007 and July 2009 distributed by CNES and CLS through the Archiving, Validation and Interpretation of Satellite Oceanographic data (AVISO) web service. This provides weekly estimates of the Absolute Dynamic Topography (ADT) for the given period, of which the temporal mean is compared to the MDTs and the mean ASAR wind corrected range Doppler velocity. The resulting ADT is, hereinafter, referred to as the AVISO ADT.

[24] The location of the NwASC (Figure 7), expressed as the maximum eastward flow at approximately 75 km from the coast, agrees well in all the data sets except the gridded drifter velocities which have significantly lower resolution, and the GOCE results which are less reliable near land. The velocity maxima and minima are largest for ASAR (31 and 26 cm/s) and least for GOCINA (16 and 11 cm/s), in both ascending (Figure 7a) and descending (Figure 7b) pass. The

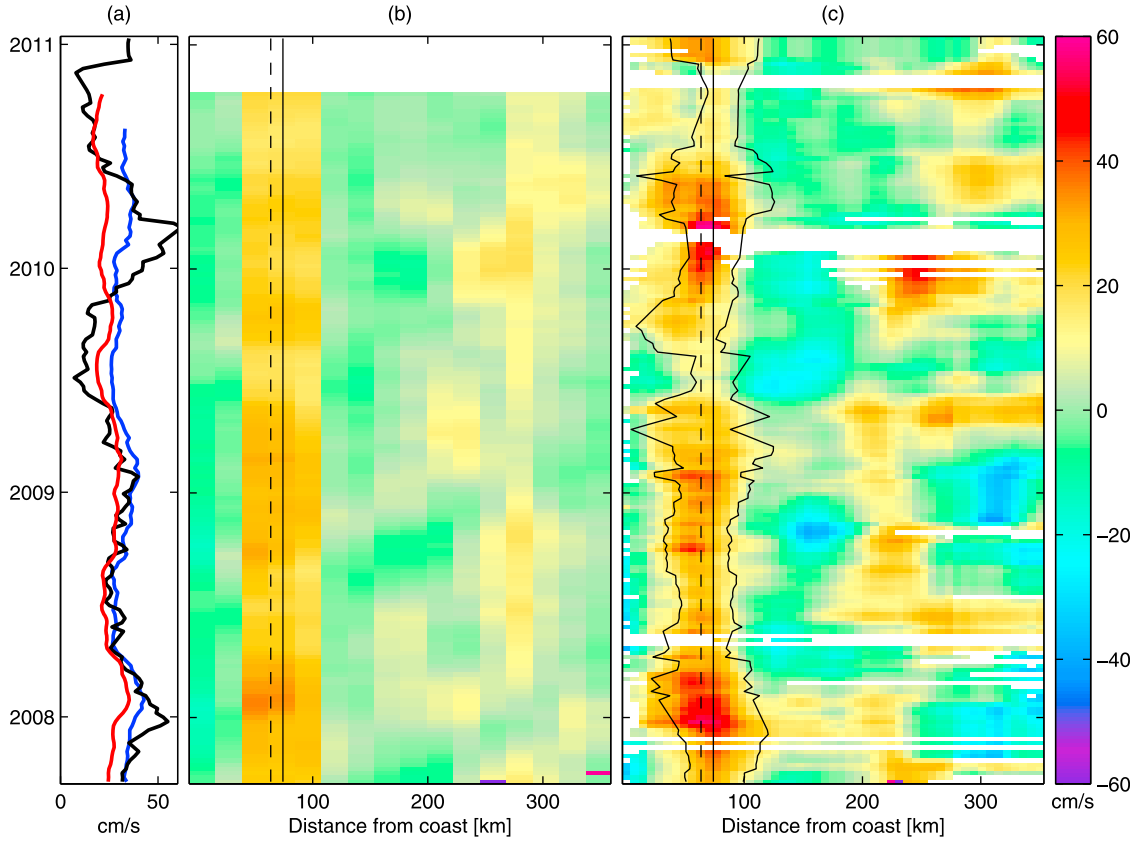

Figure 8. (a) Range velocity at S1 from the moored RCM (blue), the AVISO ADT (red), and ASAR (black), and Hovmöller diagrams across the Svinoy section from (b) AVISO and (c) ASAR in ascending satellite pass configuration from August 2007 to January 2011. The solid vertical lines in the Hovmöller diagrams mark the position of the S1 mooring, and the dashed lines mark the 200 m isobath. The white areas are missing data or data which has been removed due to RMSE of 15 cm/s or more.

CNES-CLS09 MDT and AVISO ADT, in comparison, give range velocities of 25/19 and 27/20 cm/s in ascending/descending pass, respectively.

[25] Moving further offshore, the next maximum represent the location of the NwAFC which peaks near 10 cm/s in all fields, both for ascending and descending configuration. The location of the NwAFC maximum in ascending pass (Figure 7a) is different in the ASAR data compared to the MDT results. The ASAR descending pass (Figure 7b) also reveals two minima between the NwASC and the NwAFC which are not seen in the other data. The range velocity between these minima is zero. Moreover, the ASAR, CNES-CLS09, and AVISO profiles contain west-southwestward velocities in the region between the NwASC and the NwAFC reaching up to 10 cm/s. This is an indication of recirculation which confirms previous findings of, for example, *Orvik et al.* [2001] and *Mork and Skagseth* [2010]. The overall agreement depicted in the comparison of these profiles therefore suggests that the ASAR based retrieval method capture the mean surface velocity associated with the baroclinic and barotropic contributions to the inflow of the AW to the Norwegian Sea.

[26] From these results, it is tempting to examine the seasonal variation of AW inflow across the Svinoy section from ASAR compared with current measurements from a moored RCM at 100 m depth in the Svinoy section, and the AVISO ADT. The near barotropic NwASC makes direct current measurements from the S1 mooring at 100 m depth feasible for evaluation of the ASAR measurements, although we should expect some differences especially during the presence of a more stratified upper layer in summer. The time variation at S1 and Hovmöller diagrams along the Svinoy section for the period from August 2007 to January 2011 are plotted in Figure 8 for range velocities from the three data sets: RCM, ASAR, and AVISO. All data is here low-pass filtered with a 90 days moving average, and the ASAR data represent weighted averages according to equation (3), with error estimates given by equation (4). In addition, the ASAR data is also spatially averaged over a 5 × 5 pixels neighborhood (i.e., 25 × 25 km). The average relative direction between the mean flow direction at S1 (measured by the RCM) and the radar look direction (range) is here 17°.

[27] The NwASC speed and variation at S1 (Figure 8a) agree well in all three data sets, except two enhanced winter maxima in 2008 (55 cm/s) and 2010 (62 cm/s) and a weaker summer minimum in 2009 (7 cm/s) for ASAR. The AVISO based geostrophic current is in general slightly weaker than both ASAR and the mooring measurements (except in summer 2009). The correlation between ASAR and the RCM/AVISO range velocities at this location is 0.62/0.56, with RMSDs of 9 cm/s. The corresponding correlation

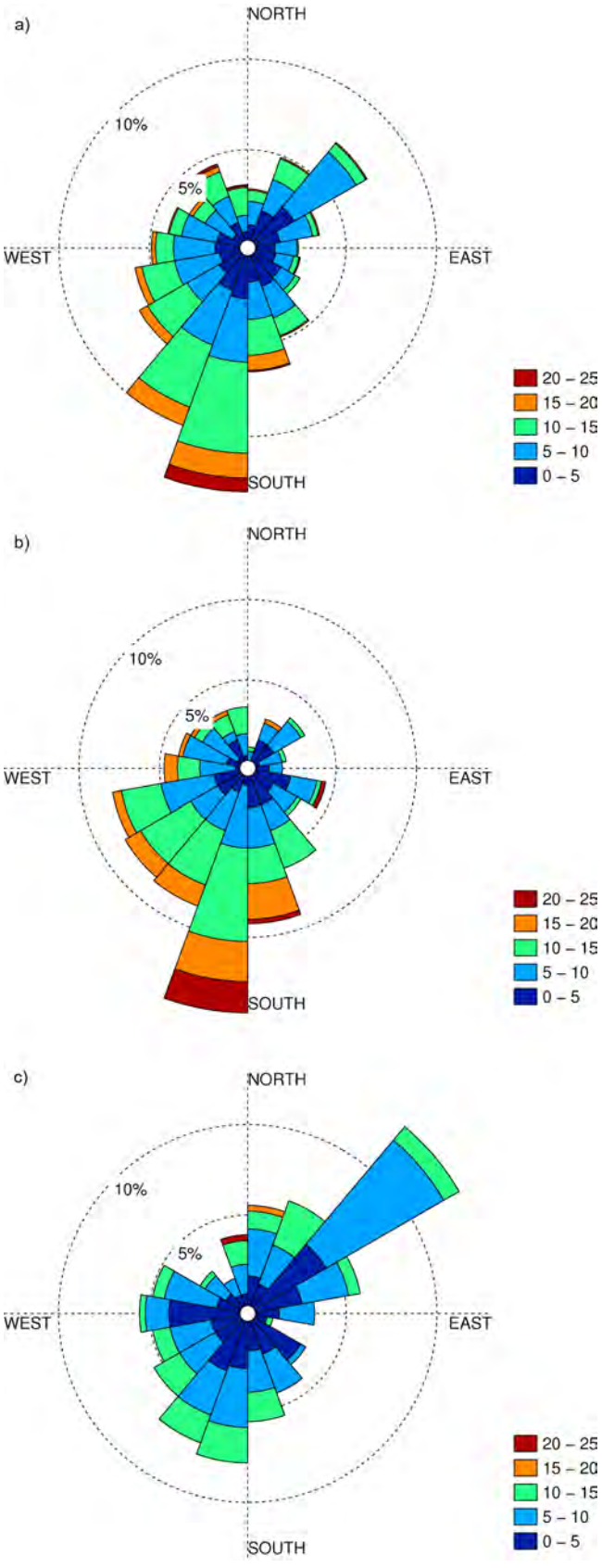

between the AVISO and RCM measurements is 0.85, with an RMSD of 6 cm/s. The locations of the NwASC and the NCC agree well in the AVISO (Figure 8b) and ASAR (Figure 8c) retrievals, except an apparent shift toward the coast in ASAR. This difference could, however, be expected from the reduced accuracy of the AVISO ADT in close proximity to land. The persistent positioning of the NwASC maximum (Figure 8c) is a clear evidence of the topographic steering along the 500 m depth contour. In contrast, the position of the NwAFC appears more variable and less clearly defined, as also found by, for example, *Mork and Skagseth* [2010], with maxima over the 1500 m to 2500 m depths meaning less steering by topography, and there is no clear seasonal variability. Its maxima are around 20 cm/s, except a strong signal approaching 40 cm/s in winter 2010. Between the NwASC and the NwAFC there is a region of mostly negative surface velocities meaning the average drift is toward west-southwest most of the year, except in winter 2008 and 2009. At the strongest, the surface velocity is here more than 20 cm/s. This surface drift pattern was also found by, for example, *Mork and Skagseth* [2010, and references therein] but of lower magnitude.

[28] The variability of the wind field in the region around S1 from August 2007 to January 2011, as shown in Figure 9a, demonstrates that south-southwesterly winds dominate. In general, this will favor northeasterly mean sea surface velocity fields as depicted in the CDOP corrected range Doppler velocity shown in Figure 2. The south-southwesterly wind regime is at the strongest during winter (Figure 9b), while it changes into northwesterly winds in summer (Figure 9c). The impact of this is also evident in the seasonal changes of the NwASC, with corresponding minima in summer and maxima in winter, as seen in Figure 8. The surface velocity in the recirculation region between the NwASC and the NwAFC in the Svinoy section also appears to be connected to the wind field as manifested, for example, by the east-northeasterly flow in winter 2008 and 2009, and west-southwesterly flow in the corresponding summers. There is, however, no clear connection between the wind field observed at S1 and the variations in the NwAFC, as the latter may be more dominated by conditions in the up-stream forcing.

[29] In the presence of baroclinicity, a clear difference should be expected between the ASAR wind corrected surface range Doppler velocity and the RCM measurements at 100 m, in particular during summer warming in the upper ocean. The correlations between ASAR and AVISO/RCM estimates are consistent with this assumption. For instance, taking the mean difference between ASAR and AVISO in Figure 8a, the contribution from nongeostrophic terms is estimated to around 4 cm/s. This, in turn, adds to the mean geostrophic current (which is 25 cm/s). Overall, these evaluation results also imply that the ASAR range surface velocity retrievals in Skagerrak and in parts of the North Sea

Figure 9. Wind roses from the Hirlam forecast model for the location of the S1 mooring (see Figure 1) from August 2007 to January 2011: the wind roses are for (a) the full period, (b) the winter months (DJF) only, and (c) the summer months (JJA) only. The wind roses indicate the direction from where the wind is blowing (meteorological convention).

Table 2. Mean Volume Flux in the NwASC[a]

	Value of k	Mean	Summer	Winter	Integration Depth	Data Source	Period
1	0.01	0.9	0.6	1.2	0–100 m	ASAR and RCM	2007–2010
2	0.1	0.9	0.7	1.2	0–100 m	ASAR and RCM	2007–2010
3	0.5	0.9	0.7	1.1	0–100 m	ASAR and RCM	2007–2010
4		4.6	3.9	5.2	full	RCM	2007–2010
5		3.4	2.4	4.7	full	hydrography, MDT	1992–2009
6		3.9			full	hydrography, gravimetry, altimetry	1993–1999
7		4.4			full	RCMs	1998-2000
8		4.2			full	hydrography, RCMs	1995–1999

[a]Measured in Sv. From the combined ASAR and RCM retrievals using different values for k (1, 2, and 3), from the RCM with a regression model from Figure 5a in the work of *Orvik and Skagseth* [2003] (4), from *Mork and Skagseth* [2010] (5), from *Hunegnaw et al.* [2009] (6), from *Orvik and Skagseth* [2003] (7), and from *Orvik et al.* [2001] (8).

can be considered reliable under these favorable imaging geometries.

[30] In combination with the RCM measurements, the volume transport in the upper layer of the inflowing AW across the Svinoy section can be estimated from the wind corrected range Doppler velocity retrievals. By assuming a constant width, L (varying from 13 km to 62 km, with a mean of 36 km, northwestward from the 200 m isobath; Figure 8), in the upper 100 m of the NwASC [*Orvik et al.*, 2001], the volume transport is calculated from

$$V_T = \left(\bar{v}_{\mathrm{RCM}} d + (\bar{v}_{\mathrm{ASAR}} - \bar{v}_{\mathrm{RCM}}) \int_0^d e^{-kz} \mathrm{dz} \right) L, \qquad (5)$$

where $\bar{v}_{\mathrm{RCM}}$ is the mean current speed at d = 100 m depth, obtained by multiplying the mean of the RCM measurements with a factor of 0.8 (which represents the ratio between the mean flow speed along L and its maximum, as obtained from ASAR), and $\bar{v}_{\mathrm{ASAR}}$ is the mean speed along L from ASAR (i.e., at the surface). Both the current speed at 100 m ($\bar{v}_{\mathrm{RCM}}$) and at the surface ($\bar{v}_{\mathrm{ASAR}}$) are projected perpendicularly to the orientation of the Svinoy section. As we cannot specify a precise value for k, we choose to examine its impact for a range of values. For k = {0.01, 0.1, 0.5}, the resulting mean volume transport in the upper 100 m is 0.9 Sv, with summer (JJA) and winter (DJF) transports of 0.6–0.7 Sv and 1.1–1.2 Sv, respectively. The volume transport estimate increases with decreasing k during winter when the ASAR estimate is higher than that of the RCM. In contrast, the transport decreases with decreasing k during summer when the ASAR estimate is lower than that of the RCM. In Table 2, these values are compared to the transport obtained from the RCM alone using a regression model presented by *Orvik and Skagseth* [2003], as well as the estimates from other studies [*Mork and Skagseth*, 2010; *Hunegnaw et al.*, 2009; *Orvik and Skagseth*, 2003; *Orvik et al.*, 2001]. These latter estimates represent the total transport in the NwASC across the Svinoy section and range from 3.4 Sv to 4.6 Sv in the mean, where the differences are largely explained by the various measurement periods as summarized in the last column of Table 2.

4. Conclusion

[31] The orientation of the two branches of the inflowing Atlantic Water (AW) in the Norwegian Atlantic Current (NwAC), and parts of the Norwegian Coastal Current (NCC), displays excellent geometry for application of the Envisat Advanced Synthetic Aperture Radar (ASAR) based range Doppler velocity method. Retrievals of the spatially and temporally varying surface velocities associated with these currents have been investigated based on 1200 ASAR Wide Swath Medium resolution image (WSM) products in VV polarization. After consistent removal of the wind driven facet motion, the Norwegian Atlantic Slope Current (NwASC) is observed with mean wind corrected range Doppler velocities from 20 to 40 cm/s, steered along the 500 m isobath with a typical width of 45 to 60 km. In comparison, the Norwegian Atlantic Front Current (NwAFC) is less distinct with lower velocities (10–15 cm/s) and a much broader core steered along the 2000–2500 m isobaths. A clear seasonal signal, including winter maxima (62 cm/s) and summer minima (7 cm/s), is found for the inflowing AW across the Svinoy section. Outside these areas of topographic steering, the surface inflow of AW diminishes. In the NCC, a narrow jet of about 40 cm/s is clearly depicted nearshore at 64°N, 9°E. In addition, the inflow/outflow to/from the Skagerrak Sea is evident in the wind corrected range Doppler velocity, with speeds reaching up to 25 cm/s. With a resolution of about 10 km, the root mean square error (RMSE) of these estimates is less than 5 cm/s.

[32] Comparison to other direct and indirect estimates of the upper ocean current, including Lagrangian drifters, moored recording current meter (RCM) measurements and surface geostrophic current inverted from several mean dynamic topographies (MDTs) ensure valuable assessment and validation. All in all, the comparison is promising, with the mean ASAR velocities slightly exceeding the other mean velocity fields. This can be expected due to better spatial resolution and contributions from the non-geostrophic terms obtained with the range Doppler velocity method. Moreover, in combination with measurements from the moored RCM, the volume transport of the inflowing AW in the upper 100 m of the NwASC across the Svinoy section was estimated with a 3-year mean transport of 0.9 Sv, and a summer minimum/winter maximum of 0.6–0.7 Sv/1.1–1.2 Sv. Compared to other full water column transport estimates of the NwASC, which average to about 4 Sv, the values are reasonable.

[33] In 2013, the European Space Agency (ESA) will launch the first Sentinel-1 C-band Synthetic Aperture Radar (SAR) mission in support of the European Global Monitoring for Environment and Security (GMES) program and future marine core services. The range Doppler velocity will then become a standard product with expected significantly better accuracies. As demonstrated in this paper, the

capability to monitor the temporal and spatial variability of the ocean surface circulation from SAR in combination with altimetry and in situ measurements will then improve, provided the imaging geometry is favorable.

[34] **Acknowledgments.** This work was supported by the Nansen Fellowship Foundation at the Nansen Environmental and Remote Sensing Center (NERSC) in Bergen, Norway, by the Research Council of Norway under contract 177441/V30, by the ESA Dragon-2 program under ESRIN contract 22494/09/I-LG, and through the ESA Changing Earth Science Network project IncuSAR. Support from the Norwegian Space Centre trough study contract 90377 is also appreciated. The altimeter products and the CNES-CLS09 MDT were produced by SSALTO/DUACS and distributed by AVISO with support from CNES. The Lagrangian drifter data was made available by the GDP of AOML in Miami, Florida, USA, and Fisheries and Oceans Canada (http://www.meds-sdmm.dfo-mpo.gc.ca). The moored RCM data was provided by K. A. Orvik at the Geophysical Institute, University of Bergen. We would also like to thank the authors of *Hunegnaw et al.* [2009] for providing their gridded drifter climatologies and MDT, Per Knudsen at DTU Space for providing the preliminary MDT from GOCE, and Even Øie Nilsen for help with Figure 1 and proofreading. Finally, we would like to thank two anonymous reviewers for constructive feedback and comments.

References

Bryden, H. L., L. M. Beal, and L. M. Duncan (2005), Structure and transport of the Agulhas Current and its temporal variability, *J. Oceanogr.*, *61*, 479–492.

Chapron, B., F. Collard, and F. Ardhuin (2005), Direct measurements of ocean surface velocity from space: Interpretation and validation, *J. Geophys. Res.*, *110*, C07008, doi:10.1029/2004JC002809.

Collard, F., A. Mouche, B. Chapron, C. Danilo, and J. A. Johannessen (2008), Routine high resolution observation of selected major surface currents from space, paper presented at SeaSAR 2008 Workshop, Eur. Space Agency, Frascati, Italy, 21–25 Jan.

Furnes, G. K., B. Hackett, and R. Saetre (1986), Retroflection of Atlantic Water in the Norwegian Trench, *Deep Sea Res., Part A*, *33*(2), 247–265.

Goldstein, R. M., and H. A. Zebker (1987), Interferometric radar measurement of ocean surface currents, *Nature*, *328*(6132), 707–709.

Gordon, R. L., and J. M. Hithnance (1987), Storm-driven continental-shelf waves over the Scottish continental shelf, *Cont. Shelf Res.*, *7*(9), 1015–1048.

Hansen, D. V., and P. M. Poulain (1996), Quality control and interpolations of WOCE-TOGA drifter data, *J. Atmos. Oceanic Technol.*, *13*(4), 900–909.

Hansen, M. W., F. Collard, K.-F. Dagestad, J. A. Johannessen, P. Fabry, and B. Chapron (2011), Retrieval of sea surface range velocities from Envisat ASAR doppler centroid measurements, *IEEE Trans. Geosci. Remote Sens.*, *49*, 3582–3592, doi:10.1109/TGRS.2011.2153864.

Hughes, C. W., and E. R. Ash (2001), Eddy forcing of the mean flow in the Southern Ocean, *J. Geophys. Res.*, *106*(C2), 2713–2722, doi:10.1029/1999JC900332.

Hunegnaw, A., F. Siegismund, R. Hipkin, and K. A. Mork (2009), Absolute flow field estimation for the Nordic Seas from combined gravimetric, altimetric, and in situ data, *J. Geophys. Res.*, *114*, C02022, doi:10.1029/2008JC004797.

Johannessen, J. A., R. A. Shuchman, G. Digranes, D. R. Lyzenga, C. Wackerman, O. M. Johannessen, and P. W. Vachon (1996), Coastal ocean fronts and eddies imaged with ERS 1 synthetic aperture radar, *J. Geophys. Res.*, *101*(C3), 6651–6667.

Johannessen, J. A., B. Chapron, F. Collard, V. Kudryavtsev, A. Mouche, D. Akimov, and K. Dagestad (2008), Direct ocean surface velocity measurements from space: Improved quantitative interpretation of Envisat ASAR observations, *Geophys. Res. Lett.*, *35*, L22608, doi:10.1029/2008GL035709.

Knudsen, P., R. Bingham, O. Andersen, and M. H. Rio (2011), A global mean dynamic topography and ocean circulation estimation using a preliminary GOCE gravity model, *J. Geod.*, *85*, 861–879, doi:10.1007/s00190-011-0485-8.

Madsen, S. N. (1989), Estimating the Doppler centroid of SAR data, *IEEE Trans. Aerospace Electronic Syst.*, *25*, 134–140, doi:10.1109/7.18675.

Maximenko, N., P. Niiler, M.-H. Rio, O. Melnichenko, L. Centurioni, D. Chambers, V. Zlotnicki, and B. Galperin (2009), Mean dynamic topography of the ocean derived from satellite and drifting buoy data using three different techniques, *J. Atmos. Oceanic Technol.*, *26*(9), 1910–1919, doi:10.1175/2009JTECHO672.1.

Mork, K. A., and O. Skagseth (2010), A quantitative description of the Norwegian Atlantic Current by combining altimetry and hydrography, *Ocean Sci.*, *6*(4), 901–911, doi:10.5194/os-6-901-2010.

Niiler, P. (2001), The world ocean surface circulation, in Ocean Circulation and Climate, Int. Geophys. Ser., vol. 77, edited by G. Siedler, J. Church, and J. Gould, pp. 193–204, Academic, San Diego, Calif.

Nilsen, J. E. O., and F. Nilsen (2007), The Atlantic Water flow along the Voring Plateau: Detecting frontal structures in oceanic station time series, *Deep Sea Res., Part I*, *54*(3), 297–319, doi:10.1016/j.dsr.2006.12.012.

Orvik, K. A., and P. Niiler (2002), Major pathways of Atlantic water in the northern North Atlantic and Nordic Seas toward Arctic, *Geophys. Res. Lett.*, *29*(19), 1896, doi:10.1029/2002GL015002.

Orvik, K. A., and O. Skagseth (2003), Monitoring the Norwegian Atlantic slope current using a single moored current meter, *Cont. Shelf Res.*, *23*(2), 159–176.

Orvik, K. A., O. Skagseth, and M. Mork (2001), Atlantic inflow to the Nordic Seas: Current structure and volume fluxes from moored current meters, VM-ADCP and SeaSoar-CTD observations, 1995–1999, *Deep Sea Res., Part I*, *48*(4), 937–957.

Poulain, P. M., A. WarnVarnas, and P. P. Niiler (1996), Near-surface circulation of the Nordic seas as measured by Lagrangian drifters, *J. Geophys. Res.*, *101*(C8), 18,237–18,258.

Rio, M. H., S. Guinehut, and G. Larnicol (2011), The new CNES-CLS09 global mean dynamic topography computed from the combination of GRACE data, altimetry and in situ measurements, *J. Geophys. Res.*, *116*, C07018, doi:10.1029/2010JC006505.

Romeiser, R., and D. R. Thompson (2000), Numerical study on the along-track interferometric radar imaging mechanism of oceanic surface currents, *IEEE Trans. Geosci. Remote Sens.*, *38*, 446–458.

Romeiser, R., J. A. Johannessen, B. Chapron, F. Collard, V. Kudryavtsev, H. Runge, and S. Suchandt (2010), Direct surface current field imaging from space by along-track insar and conventional sar, in *Oceanography from Space Revisited*, edited by V. Barale, J. F. R. Gower, and L. Alberotanza, pp. 73–91, Springer, New York.

Rouault, M. J., A. Mouche, F. Collard, J. A. Johannessen, and B. Chapron (2010), Mapping the Agulhas Current from space: An assessment of ASAR surface current velocities, *J. Geophys. Res.*, *115*, C10026, doi:10.1029/2009JC006050.

Skagseth, O., and K. A. Orvik (2002), Identifying fluctuations in the Norwegian Atlantic Slope Current by means of empirical orthogonal functions, *Cont. Shelf Res.*, *22*(4), 547–563.

Skagseth, O., K. A. Orvik, and T. Furevik (2004), Coherent variability of the Norwegian Atlantic slope current derived from TOPEX/ERS altimeter data, *Geophys. Res. Lett.*, *31*, L14304, doi:10.1029/2004GL020057.

Søiland, H., M. D. Prater, and T. Rossby (2008), Rigid topographic control of currents in the nordic seas, *Geophys. Res. Lett.*, *35*, L18607, doi:10.1029/2008GL034846.

Sætre, R. (Ed.) (2007), *The Norwegian Coastal Current—Oceanography and Climate*, Tapir Acad. Press, Trondheim, Norway

Taylor, J. R. (1997), *An Introduction to Error Analysis: The Study of Uncertainties in Physical Measurements*, Univ. Sci. Books Herndon, Va.

B. Chapron, Laboratoire d'Océanographie Spatiale, Institut Francais de Recherche pour l'Exploitation de la Mer, F-29280 Plouzané, France.

F. Collard, Collecte Localisation Satellites, 115 Rue Claude Chappe, F-29280 Plouzané, France.

K. F. Dagestad, M. W. Hansen, and J. A. Johannessen, Nansen Environmental and Remote Sensing Center, Thormøhlens Gate 47, N-5006 Bergen, Norway. (morten.hansen@nersc.no)